Journal of Hazardous Materials 190 (2011) 604–612

Contents lists available at ScienceDirect

Journal of Hazardous Materials

journal homepage: www.elsevier.com/locate/jhazmat

Efficient visible light driven photocatalytic removal of NO with aerosol flow synthesized B, N-codoped TiO_2 hollow spheres

Xing Ding, Xiao Song, Pengna Li, Zhihui Ai, Lizhi Zhang*

Key Laboratory of Pesticide & Chemical Biology of Ministry of Education, College of Chemistry, Central China Normal University, Wuhan 430079, People's Republic of China

ARTICLE INFO

Article history:
Received 28 November 2010
Received in revised form 24 March 2011
Accepted 24 March 2011
Available online 6 April 2011

Keywords:
Boron
Nitrogen
Codoped
TiO_2
Photocatalysis
NO removal

ABSTRACT

In this study, we demonstrate that aerosol assisted flow synthesized B, N-codoped TiO_2 photocatalyst possesses superior photocatalytic activity to pure and single element doped counterparts on the degradation of NO in a flow system under both simulated solar light and visible light irradiation. Characterization results revealed that B, N-codoped TiO_2 photocatalyst was composed of hollow microspheres. Boron and nitrogen were in the form of Ti–O–B and N–Ti–O structures, respectively. The introduction of B and N into the TiO_2 lattice could effectively tune the band gap of TiO_2 and extend its optical response to the visible-light region. The synergistic effect of B and N codoping on visible light driven photocatalytic activity enhancement of TiO_2 was discussed on the basis of experimental results.

1. Introduction

Nitric oxide (NO) exhausted from internal combustion engines and furnaces is a kind of harmful air pollutants which can cause photochemical smog, acid rain, greenhouse effects and so on [1]. Recently, scientists have paid more and more attention to air quality with increasing awareness of the public environment and health, especially in urban cities [2]. Photocatalysis is an increasingly attractive method for both atmospheric and aquatic purification [3]. Among all the photocatalysts, TiO_2 is the most widely used photocatalyst for the purpose of environmental purification [4,5]. However, TiO_2 has a relatively large band gap of 3.0–3.2 eV. Hence, it can only be activated under UV light irradiation [6], which constitutes only a small fraction (about 3–5%) of the solar spectrum. One of the most important and challenging issues is to develop efficient visible light sensitive photocatalysts by the modification of TiO_2. The initial approach is to dope TiO_2 with transition metal elements [7,8]. However, transition metal ion-doped TiO_2 suffers from some serious drawbacks, such as thermal instability and low quantum efficiency of the photoinduced charge carriers [9]. Another approach is to dope TiO_2 with nonmetal atoms. For instance, the doping of nitrogen [10,11], carbon [12,13], sulfur [14] and iodine [15] in TiO_2 can lower its band gap and shift its optical response to the visible light region because the related impurity states are near the valence band edge, which could minimize their possibility as recombination centers compared to metal doping [16]. Little is known about boron-doped TiO_2 in comparison with other nonmetals, and the controversial phenomena were observed on the boron-doped TiO_2 prepared by different groups. For example, Zhao et al. [17] and In et al. [18] found that B-doped TiO_2 samples synthesized by a modified sol–gel method showed a red-shifted absorption spectrum. On contrary, Chen et al. [19] found that the band gap of B-doped TiO_2 synthesized by using titanium tetra-*n*-butyl oxide (TTB) and H_3BO_3 increased because of the decrease of the crystal size after boron doping. Besides, Bettinelli et al. [20] found that the addition of B could favor the transformation of anatase to rutile for TiO_2 when using modified sol–gel processes. Fittipaldi et al. [21] found that the behavior of the EPR signals might be interpreted in terms of a sensitization of the B-doped TiO_2 prepared by a sol–gel method with titanium(IV) butoxide to visible light, although its band gap was very large. Finazzi et al. [22] reported that B in the bulk of anatase could undertake different positions and give rise to very different situations on the electronic structure of boron-doped anatase TiO_2 according to the results of density functional theory calculations. These research results suggest the doping mode of boron in TiO_2 highly depends on the preparation methods.

More recently, the simultaneous doping of two or three kinds of atoms into TiO_2, such as C–N–TiO_2 [23], C–S–TiO_2 [24], N–F–TiO_2 [25,26], F–B–TiO_2 [27] and C, N and S-tridoped TiO_2 [28], has attracted considerable interest because it can result in a higher

* Corresponding author. Tel.: +86 27 6786 7535; fax: +86 27 6786 7535.
E-mail address: zhanglz@mail.ccnu.edu.cn (L. Zhang).

0304-3894/$ – see front matter © 2011 Elsevier B.V. All rights reserved.
doi:10.1016/j.jhazmat.2011.03.099

photocatalytic activity and unusual characteristics compared with single element doping. B, N-codoped TiO_2 photocatalyst was first reported by Lambert and co-workers [18] via the sequential reaction of BH_3 in THF with a calculated small excess of $TiCl_4$ under a dry, O_2-free nitrogen atmosphere in 2007. Then, sol–gel method [29–31] and two-step hydrothermal process [32] was used to prepare B, N-codoped TiO_2 powders with enhanced visible-light absorption and high activity in the visible region. Obviously, all these procedures involved complex steps, and required long time, high cost, and rigorous condition, and/or generated pollutants from the oxidation/decomposition of the surfactants. Therefore, the seeking of new facile approaches to synthesize codoped TiO_2 is of increasing interest. Aerosol assisted flow synthetic method is a versatile technique for producing ceramic materials on the industrial scale with a wide variety of particle morphologies, sizes, and compositions [33]. A distinctive feature of these sprayed powders is the homogeneous distribution of constituents throughout all of the particles because all of the constituents are formed from a solution [34]. Previously, we have successfully prepared metal oxides hollow spheres [35] and B, Ni-codoped TiO_2 [36] with one-step aerosol assisted flow synthetic method. The as-prepared B, Ni-codoped TiO_2 photocatalysts were hollow spheres and exhibited high photocatalytic activity on the degradation of NO under simulated solar light irradiation.

In this study, we demonstrate that aerosol flow synthesized B, N-codoped TiO_2 photocatalyst possesses superior photocatalytic activity to the counterpart single element doped TiO_2 products on the degradation of NO in a flow system under simulated solar light and visible light irradiation. The synergistic effect of B and N codoping on visible light driven photocatalytic activity enhancement of TiO_2 was studied in detail.

2. Experimental

2.1. Sample preparation

All of the reagents used in this study were of analytical grade and used without further purification. Titanium tetrachloride ($TiCl_4$) was purchased from Shanghai China. Boric acid (H_3BO_3) and urea were purchased from Shanghai Chemical Reagent Limited Company and Guangdong Taishan Chemical Reagent Factory, respectively. Commercial photocatalyst P25 (a mixture of 80% anatase and 20% rutile) was purchased from Degussa (Germany). B-doped, N-doped, and B, N-codoped photocatalysts were all synthesized by an aerosol-assisted flow synthetic method (Scheme S1, Supporting Information) using H_3BO_3 and urea as the B and N sources, respectively. For the B, N-codoped TiO_2 photocatalyst, urea (10 mmol), H_3BO_3 (10 mmol) and $TiCl_4$ (10 mmol) were dissolved into 80 mL of distilled water at 0 °C under stirring. The resulting solutions were nebulized using an ultrasonic nebulizer at 1.7 MHz ± 10% (YUYUE402AI, Shanghai) and then carried by an air flow through a quartz tube surrounded by a furnace thermostated at 600 °C for 1 h under an ambient temperature of around 25 °C. The quartz reaction tube with the diameter of 3.5 cm was 1 m long. The products were collected in a percolator with distilled water, then filtered by a fritted glass funnel, washed thoroughly with distilled water and ethanol, and finally dried in an oven at 60 °C. The yield of the BNT sample was around 95%. The preparations of B-doped and N-doped TiO_2 were similar with that of B, N-codoped TiO_2 by adding only H_3BO_3 or urea. Pure TiO_2 was synthesized without the addition of H_3BO_3 and urea into the precursor solution with the same procedure. Pure TiO_2, B-doped TiO_2, N-doped TiO_2 and B, N-codoped TiO_2 were designated as PT, BT, NT and BNT, respectively.

2.2. Characterization

The powder X-ray diffraction (XRD) measurements were carried out using a Rigaku D/MAX-RB diffractometer with monochromatized Cu K radiation ($\lambda = 0.15418$ nm). Transmission electron microscopy (TEM) images were taken with a JEOL JSM-2010 electron microscopy instrument. The samples for TEM were prepared by dispersing the final powders in ethanol with ultrasonic irradiation, the dispersion was then dropped on carbon–copper grids. Scanning electron microscopy (SEM) images were observed by a JEOL 6700-F electron microscopy instrument. The Brunauer–Emmett–Teller (BET) surface areas of the powder samples were determined by nitrogen adsorption–desorption isotherm measurements at 77 K on a Micromeritics Tristar-3000 nitrogen adsorption apparatus. The UV–vis diffuse reflectance spectra (DRS) of the samples were measured in the range of 200–800 nm using a UV–vis spectrometer (UV-2550, Shimadzu) with $BaSO_4$ as a reference. X-ray photoelectron spectroscopy (XPS) measurements were performed in a VG Scientific ESCALAB Mark II spectrometer equipped with two ultra-high vacuum (UHV) chambers. All binding energies were referenced to the C 1s peak at 284.6 eV of the surface adventitious carbon.

2.3. Photocatalytic NO removal

The photocatalytic experiments for the removal of NO in air were performed at ambient temperature in a continuous flow reactor. The volume of the rectangular reactor which was made of stainless steel and covered with Saint-Glass was 4.5 L (10 cm × 30 cm × 15 cm ($H \times L \times W$)). One sample dish containing the 0.2 g catalyst powders was placed in the middle of the reactor. A 300 W commercial tungsten halogen lamp (General Electric) was used as the simulated solar light source because the light from tungsten halogen lamp contains both UV light and visible light. To obtain visible light, we remove the UV light with a glass filter whose transmissivity of the UV zone (200–420 nm) was less than 1%. The lamp was vertically placed outside the reactor above the sample dish. Four mini-fans were fixed around the lamp to avoid the temperature rise of the flow system. The integrated UV intensity in the range of 310–400 nm measured by Digital Radiometer (DRC-100X, SPECTROLINE) was $720 \pm 10\ \mu W/cm^2$. The catalyst sample was ready for test by coating an aqueous suspension of our sample onto the dish with a diameter of 12.0 cm, the irradiated area of the samples was about 113 cm^2. The dishes containing the photocatalyst were pretreated at 60 °C for water evaporation and then cooled to room temperature for photocatalytic NO removal. NO gas was selected as the target pollutant for the photocatalytic degradation at ambient temperature. The NO gas was acquired from a compressed gas cylinder at a concentration of 48 ppm NO (N_2 balance, BOC gas) with traceable National Institute of Standards and Technology (NIST) standard. The initial concentration of NO was diluted to about 400 ppb by the air stream supplied by a zero air generator (Thermo Environmental Inc. model 111). The desired humidity level of the NO flow was controlled at 70% (2100 ppmv) by passing the zero air streams through a humidification chamber. The gas streams were premixed completely by a gas blender, and the flow rate was controlled at 4 L/min by a mass flow controller (MODEL FC-260, TYLAN Corp.). After the adsorption–desorption equilibrium among water vapor, gases, and photocatalysts was achieved, the lamp was turned on. The concentration of NO was continuously measured by a chemiluminescence NO analyzer (Thermo Environmental Instruments Inc. model 42c), which monitors NO, NO_2, and NO_x (NO_x represents $NO + NO_2$) with a sampling rate of 0.7 L/min.

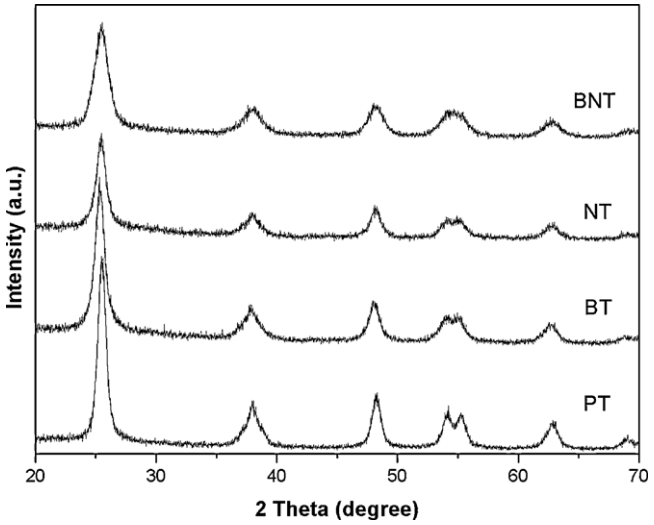

Fig. 1. XRD patterns of the pure (PT); B-doped (BT), N-doped (NT) and B, N-codoped TiO_2 (BNT).

The removal efficiency (η) of NO was calculated as follows.

$$\eta(\%) = \left(1 - \frac{C}{C_0}\right) \times 100\%$$

where C and C_0 were the concentrations of NO in the outlet stream and the feeding stream, respectively.

3. Results and discussion

3.1. XRD patterns

XRD was used to investigate the phase structures and crystallite size of the aerosol flow synthesized powders (Fig. 1). The diffraction peaks of all the samples could be indexed to anatase phase (JCPDS, file No. 21-1272). According to the line width analysis of the (1 0 1) diffraction peak based on the Scherrer formula, the average crystallite sizes for PT, BT, NT, and BNT were 9.8, 10.5, 8.4 and 6.4 nm, respectively. Compared with PT, the crystal size of BT increased, which was consistent with the literature [37], because the introduction of residual charge after B doped may lead to the increase of surface O–H groups and crystal size [40]. In contrast, the size of NT decreased because dissimilar boundaries provided the single doping of nitrogen could inhibit the crystal growth. The crystal size of BNT decreased more significantly in comparison with NT. This decrease might be ascribed to dopant-induced distortions and more dissimilar boundaries arisen from the synergistic effect of codoping of boron and nitrogen because of the existence of the internal B–O–Ti–N structure [38], which will be discussed later.

3.2. SEM and TEM images

The as-prepared products were further analyzed by SEM and TEM measurements. Both PT (Fig. 2a) and NT (Fig. 2b) were spherical in shape according to the SEM images. We could clearly observe that lots of hollow structured microspheres existed in both BT (Fig. 2c) and BNT (Fig. 2d) samples. The TEM images reveal that PT and NT consist of plenty of spheres (Fig. 3a and b). But we did not observe any hollow spheres in PT and NT. As shown in Fig. 3c and d, the strong contrast between the dark edge and bright center obviously confirms the existence of hollow nature. The produced microspheres were composed of a hollow inner cavity and thin outer shell. The thickness of the microspheres shells was very thin and therefore we can observe some shrinkage on the surface of BT and BNT samples. In addition, a few fragments could be found during the TEM observation, indicating that the spheres were not very compact and some of them may be destroyed by intensive postsonication or inner expansibility. Therefore, the boron dopant might play an important role for the formation of hollow structure. The formation mechanism has been discussed in our previous paper in detail [35], which is only shown in Supporting Information in this study.

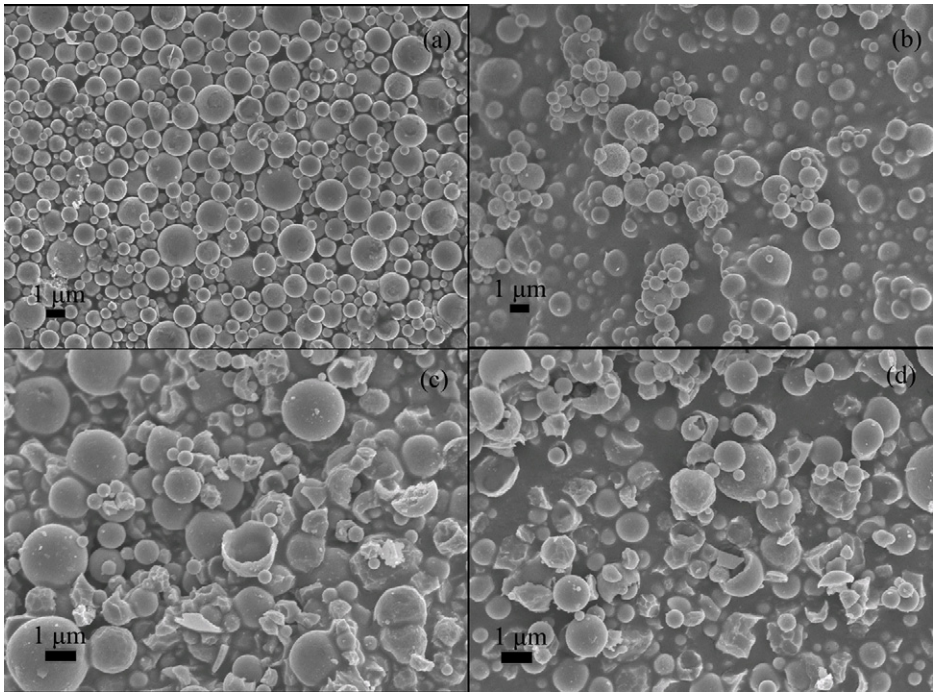

Fig. 2. SEM images of the resulting samples prepared by the aerosol-assisted flow synthetic method. (a) PT; (b) NT; (c) BT; and (d) BNT.

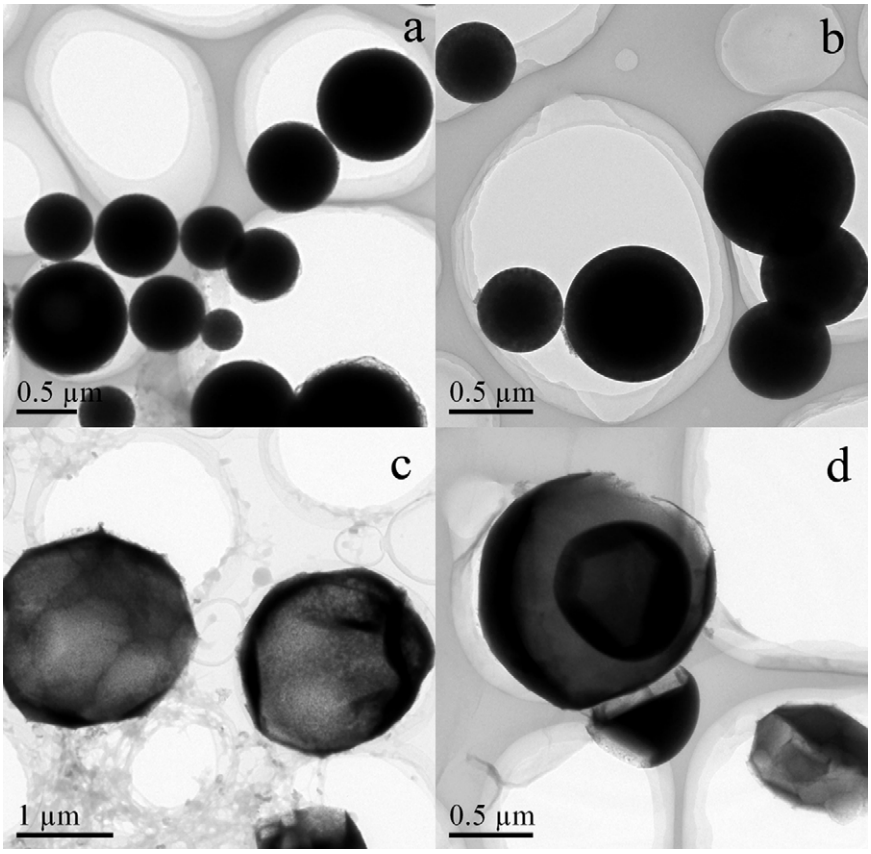

Fig. 3. TEM images of the resulting samples prepared by the aerosol-assisted flow synthetic method. (a) PT; (b) NT; (c) BT; and (d) BNT.

3.3. The nitrogen adsorption–desorption analysis

The nitrogen adsorption–desorption isotherms and pore size distribution curves of the as-prepared samples were also recorded (Fig. 4). All the samples exhibited the type IV isotherm with an H3 type hysteresis loop [39], suggesting the mesoporous structures in the resulting materials. These mesopores should be formed by the agglomeration of TiO_2 nanocrystals. The BET specific surface areas for the samples PT, BT, NT and BNT were 30, 134, 31, and 182 m^2/g, respectively. Obviously, the presence of H_3BO_3 could significantly enhance the surface area of the sample. The surface area (134 m^2/g) of hollow structured BT sample was nearly 4.3 times of that of PT powders (30 m^2/g). With the coexistence of N and B in TiO_2, the surface area was increased to 182 m^2/g, about 6 times of that of PT powders. The larger surface area and pore diameter of BT and BNT hollow spheres should be caused by the in situ emission of HBO_2 gas from the decomposition of H_3BO_3 during the formation of TiO_2 spheres [35,36]. The surface area of NT (31 m^2/g) was just slightly larger than of PT (30 m^2/g), suggesting the addition of urea did not contribute much to the surface area enhancement. This may be attributed to the earlier decomposition of urea before the formation of spheres.

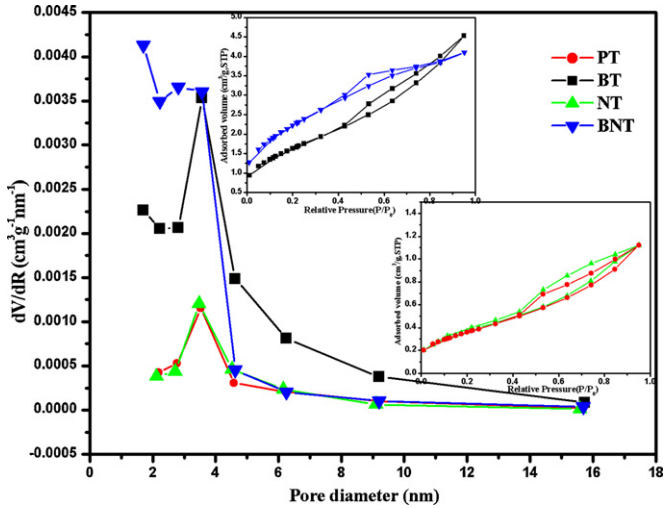

Fig. 4. The nitrogen adsorption–desorption isotherms (inset) and pore size distribution curves of the as-prepared samples.

3.4. UV–vis spectra

The UV–vis diffuse reflectance spectra of the resulting samples showed that the absorption edge position of BT moved toward shorter wavelength in comparison with PT, suggesting that the band gap of TiO_2 increased after boron doping (inset of Fig. 5), which might be ascribed to the existence of tricoordinated borons [40] and the Ti–O–B structure in boron doped TiO_2 [32] as reported previously. The spectra of NT and BNT extended a red shift and their absorbance in the visible range from 400 to 600 nm increased. As TiO_2 is an indirect transition semiconductor, plots of the $(\alpha h\nu)^{1/2}$ (α is the absorption coefficient, and $h\nu$ is the photon energy) vs the energy of absorbed light afford the band gaps of as-prepared samples. As shown in Fig. 5, the band gaps obtained in such a way were approximately 2.91, 3.03, 2.66, 2.77 and 3.01 eV for the sample PT, BT, NT, BNT and P25, respectively. The red shift of NT and BNT is owing to the doping of N because the hybridiza-

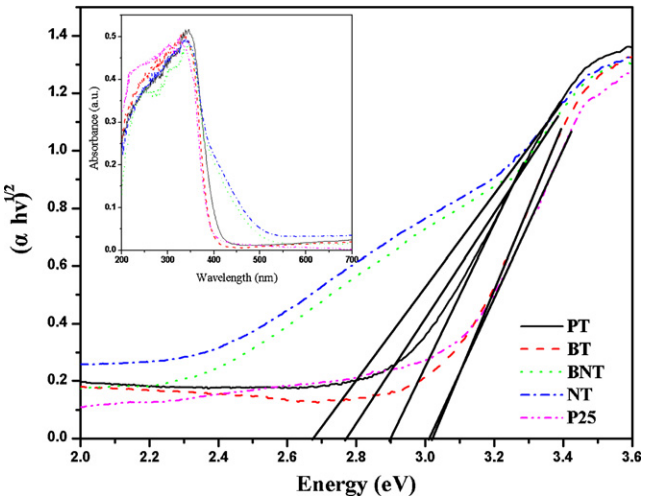

Fig. 5. Plots of the $(\alpha h\nu)^{1/2}$ vs the energy of absorbed light and UV–vis diffuse reflectance spectra (inset) of P25, BT, PT, NT and BNT.

tion of p states of N with O2p state could result in the band gap narrowing [10].

3.5. XPS analysis

XPS was used to investigate the surface element composition of the as-prepared samples (Fig. 6). The survey spectra in Fig. 6a indicate that BNT sample contain O, B, N, Ti and certain amounts of C from precursor solution and the adventitious hydrocarbon in the XPS instrument itself. The high-resolution XPS spectra of the sample were also recorded. Fig. 6 reveals that N 1s peaks cannot be observed on the XPS spectra of sample PT and BT, while there are no B 1s signal on the spectra of PT and NT. It is observed that the B 1s region contains only one peak with the binding energy at 191.7 eV for BNT (Fig. 6b). As compared to the standard binding energy for B 1s in B_2O_3 (193.1 eV, B–O bonds) and in TiB_2 (187.5 eV, Ti–B bonds), this binding energy of B 1s in BNT was between that of B_2O_3 and TiB_2. Therefore, the peak at 191.7 eV probably corresponds to boron embedded into the interstitial TiO_2 structure, existing in the form of Ti–O–B structure [19]. For the BT sample, the B 1s region contains only one peak with the binding energy at 191.6 eV, which also confirms the formation of Ti–O–B structure. As for N, only one peak with the binding energy at 399.7 eV is obtained by fitting curves for BNT (Fig. 6c). The assignment of the N 1s peak around 400 eV is still controversial and under debate. It may be attributed to ammonia, nitrogen or the anionic N^- in O–Ti–N linkages [10,41,42]. Usually, the XPS peak related to ammonia is a little above 400 eV [43]. Meanwhile, in this study the existence of ammonia in TiO_2 is almost impossible for its high solubility in water. And the assignment of the N 1s peak to chemisorbed molecular N_2 is implausible as well because N_2 is not easily chemisorbed on TiO_2 at room temperature. From Fig. 6c, the fact that the peaks around 400 eV only exist in the spectra of NT and BNT but not in those of BT and PT also rules out the possibility of N_2 chemisorptions. So we conclude that the peak with the binding energy at 399.7 eV is due to the existence of anionic N^- in O–Ti–N linkages and N atoms might be incorporated into the TiO_2 crystal lattice with a form of substitution [38,44]. For the NT sample, the N 1s region contains only one peak with the binding energy at 399.6 eV, similar to that of BNT. Lu and his co-workers proposed the formation of O–Ti–B–N structure on the surface of the B, N-codoped TiO_2 sample due to nitridation [32], where new peaks with binding energies of 190.0 and 397.7 eV appear in the B 1s and N 1s spectra, respectively. However, in this work no peaks with binding energies of 190.0 and 397.7 eV were observed in the B 1s and N 1s spectra of BNT samples. Therefore, we deduce that the B–N structure could not exist in BNT sample and a novel B–O–Ti–N structure might be formed in the B, N-codoped TiO_2 obtained by the aerosol assisted flow synthetic method. In addition, the XPS spectrum of $Ti2p_{3/2}$ in the sample BNT can be fitted as one peak at 458.3 eV which shows a red-shift of 0.23 eV compared to the binding energy of Ti^{4+} in pure TiO_2 (Fig. 6d), suggesting that the electronic interaction of Ti with anions in sample BNT is different from that in TiO_2 [45] and partial existence of Ti^{3+} in BNT [19]. The XPS spectrum of C 1s of the four samples could be fitted with two peaks at 284.6 eV and 286.8 eV (Fig. 6e). Wu and co-workers [46] synthesized mesoporous C-doped titanium dioxide in 2009 and found the peak of the O–Ti–C bond appeared at 282.4 eV, which did not exist in the C 1s spectra in Fig. 6e. Therefore, we assigned the peaks at 284.6 eV and 286.8 eV to the residual carbon from precursor solution and the adventitious hydrocarbon, respectively.

3.6. Formation mechanism of hollow microspheres

We believe the formation process of B, N-codoped TiO_2 hollow microspheres is similar to that of B doped TiO_2 hollow spheres and B, Ni-codoped TiO_2 [35,36]. It is known that the aerosol assisted flow synthetic process generally involves several stages: atomization, solvent evaporation and solute precipitation, drying, precursor decomposition, calcinations, and particle shaping. It is widely believed that the drops, when sprayed into a tubular reactor under pyrolysis conditions, serve as micro-reactors and yield one particle per drop during the aerosol flowing. According to the one particle per drop rule, in our study each drop served as a micro-reactor containing $TiCl_4$ precursor and H_3BO_3 as well as water. The temperature of the drop varied as it traveled with the flowing aerosol along the high temperature furnace tube. As the water evaporated, the diameter of the precursor drop decreased, and the titanium precursor concentration increased. Eventually, the titanium precursor drop was completely dehydrated, and the hydrolysis of $TiCl_4$ produced hydrous TiO_2 and thus TiO_2 spheres were subsequently formed in the flowing aerosol. During the formation of TiO_2 spheres, the decomposition of H_3BO_3 would proceed simultaneously and/or subsequently in the droplet under high temperature, producing HBO_2 which is volatile at 600 °C. The resulting HBO_2 gas would escape from the TiO_2 spheres to create hollow inner structures. The formation process was illustrated by Scheme S2 in the Supporting Information.

3.7. Photocatalytic activities

The ability of the as-prepared samples to remove NO was investigated in order to evaluate their potential for air purification. In the presence of the as-prepared samples, the nitrogen monoxide reacted with reactive radicals and produced HNO_2 and HNO_3, which involved four reactions displayed in Eqs. (1)–(4) [47].

$$NO + 2^{\bullet}OH \rightarrow NO_2 + H_2O \quad (1)$$

$$NO_2 + {}^{\bullet}OH \rightarrow NO_3^- + H^+ \quad (2)$$

$$NO + NO_2 + H_2O \rightarrow 2HNO_2 \quad (3)$$

$$NO + {}^{\bullet}O_2^- \rightarrow NO_3^- \quad (4)$$

Fig. 7 shows the NO concentration changes vs irradiation time in the presence of the aerosol flow synthesized samples. It was found that the photolysis of NO in the absence of photocatalysts was negligible under both simulated solar light and visible light irradiation. After 30 min of degradation under simulated solar light irradiation (Fig. 7a), 4, 31, 45, 12, and 53% of NO were photocatalytically oxidized on the samples of P25, PT, BT, NT and BNT, respectively.

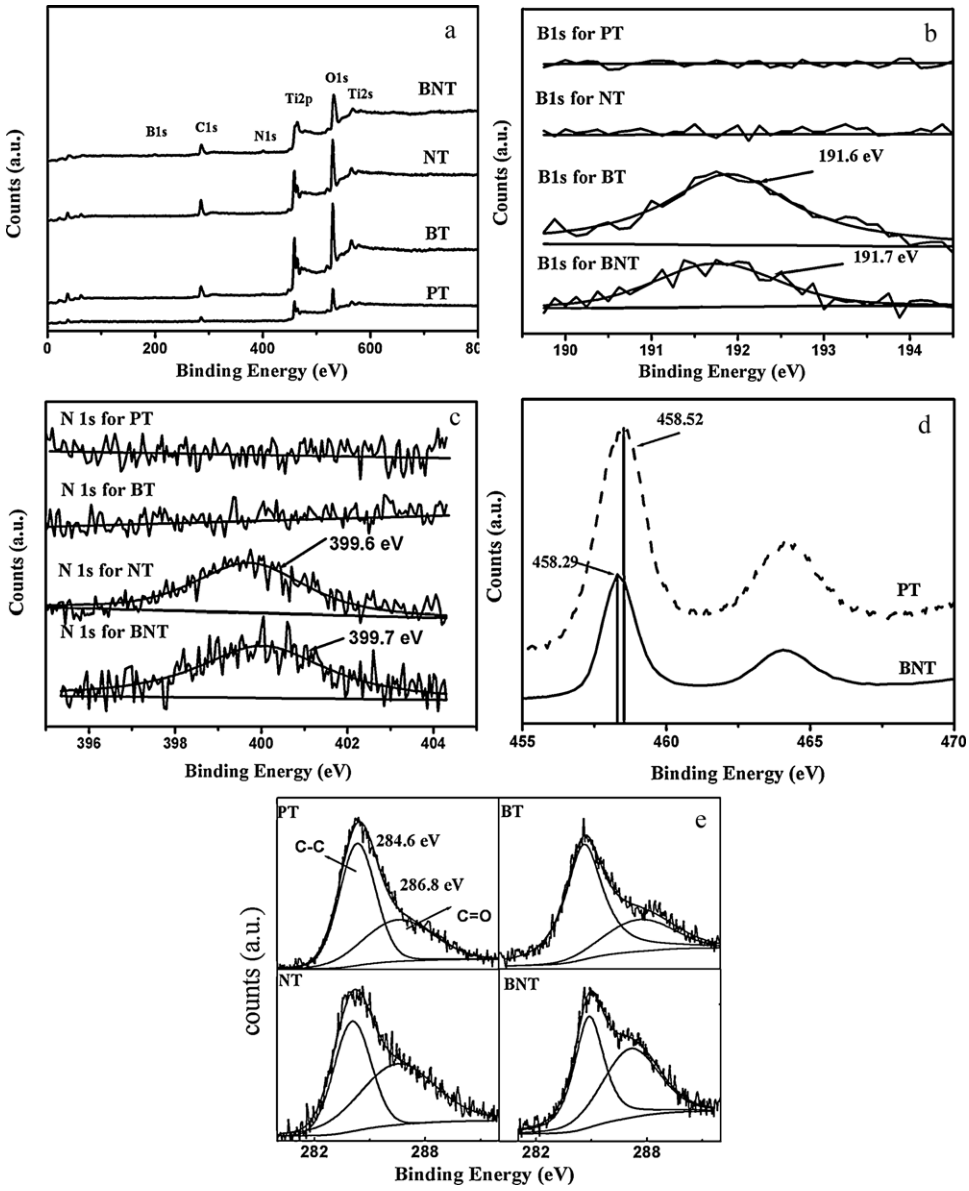

Fig. 6. XPS spectra of PT, NT, BT and BNT samples obtained by the aerosol-assisted flow synthetic method (a); the high-resolution XPS spectra of the B 1s of PT, BT, NT and BNT (b); N 1s of PT, BT, NT and BNT (c); Ti2p of PT and BNT (d); and C 1s of PT, BT, NT and BNT (e).

Moreover, the simulated solar light driven photocatalytic activity of the BNT photocatalyst was even significantly higher than that of nonaqueous sol–gel synthesized BiOBr (45% NO removal in 30 min) in our group [47].

Under the simulated solar light irradiation, the NO degradation over PT could reach 31%. This is because it could be activated by the UV light in simulated solar light. For the sample BT, although the band gap of BT was enlarged to 3.03 eV, it could still be activated under the simulated solar light. We believe the enlargement of band gap by boron doping could enhance photocatalytic activity of BT. Generally, a larger band gap corresponds to a more powerful redox ability and a higher energy level of the conduction band [48], which could favor the production of active oxygen radicals (e.g., $\bullet O_2^-$, •OOH, •OH) [49], and thus enhance the oxidation of NO. Therefore, the band gap difference could explain the higher photocatalytic activity of BT and the lower photocatalytic activity of NT in comparison with PT under simulated solar light irradiation. The lower visible light activity of NT should be attributed to high photo-generated electrons and holes recombination rates because of its small band gap and crystal defects induced by single nitrogen doping.

Under the visible light irradiation, the photocatalytic activity of the four aerosol flow synthesized samples decreased largely because of the removal of UV light, as shown in Fig. 7b. The removal efficiencies were about 1, 5, 9, 4 and 24% for P25, PT, BT, NT and BNT, respectively. The photocatalytic efficiencies of P25, PT, BT, NT and BNT under visible light were 25%, 16%, 20%, 33%, and 45% of those under simulated solar light irradiation. Obviously, the as-prepared BNT photocatalyst could more effectively remove NO even under visible light than single doped BT and NT. We think the notable photocatalytic activity enhancement of B, N-codoped TiO_2 in comparison with single N or B-doped TiO_2 could be attributed to its high surface area, abundant mesoporous structure, narrow band gap energy, and remarkable synergetic effect of boron and nitrogen dopants because of the existence of B–O–Ti–N structure(Table 1). First, the XRD and N_2 sorption characterizations revealed that the crystal size of BNT decreased and its surface area increased significantly after the codoping of boron and nitrogen into TiO_2. As

Table 1
Summary of physicochemical properties of pure TiO_2 (PT), B-doped TiO_2 (BT), N-doped TiO_2 (NT), B, N-codoped TiO_2 (BNT) and P25.

Sample	Crystal size (nm)	S_{BET} (m^2/g)	Pore diameter (nm)	Band gap (eV)	NO degradation efficiency under simulated solar light (%)	NO degradation efficiency under visible light (%)
P25	20–30	50	–	3.01	4	1
PT	9.8	30	3.4	2.91	31	5
BT	10.5	134	3.6	3.03	45	9
NT	8.4	31	3.4	2.66	12	4
BNT	6.4	182	3.6	2.77	53	24

expected, this larger surface area will lead to a higher photoactivity, because larger surface could provide more active sites and generate more reactive species [50,51]. Second, the transport of NO through the interior space can be feasible because of the mesoporous structure of the as-prepared BNT samples. The porous structure could also facilitate the harvesting of visible light due to the enlarged surface area [46]. Third, although the band gap of BT increased with the doping of boron into TiO_2, the band gap of BNT decreased after N was further doped to form the B–O–Ti–N structure (Fig. 5). The red shift in the band gap transition of the BNT sample indicated that more photo-generated electrons and holes can participate in the photocatalytic reactions under visible light irradiation, which can enhance the visible light driven photocatalytic activity of TiO_2. Fourth, partial Ti^{3+} was generated due to the boron doping by charge compensation [19,52], which lead to the formation of the defects (e.g., oxygen vacancies) to trap the photogenerated electron and enhance the final photocatalytic activity. Lastly, the charge compensation between B (3+) and N (1−) through an internal charge transfer with a large stabilization effect in the B, N-codoped TiO_2 largely reduced the photo transition energy from the valence band to the conduction band, resulting in a higher photocatalytic activity [53].

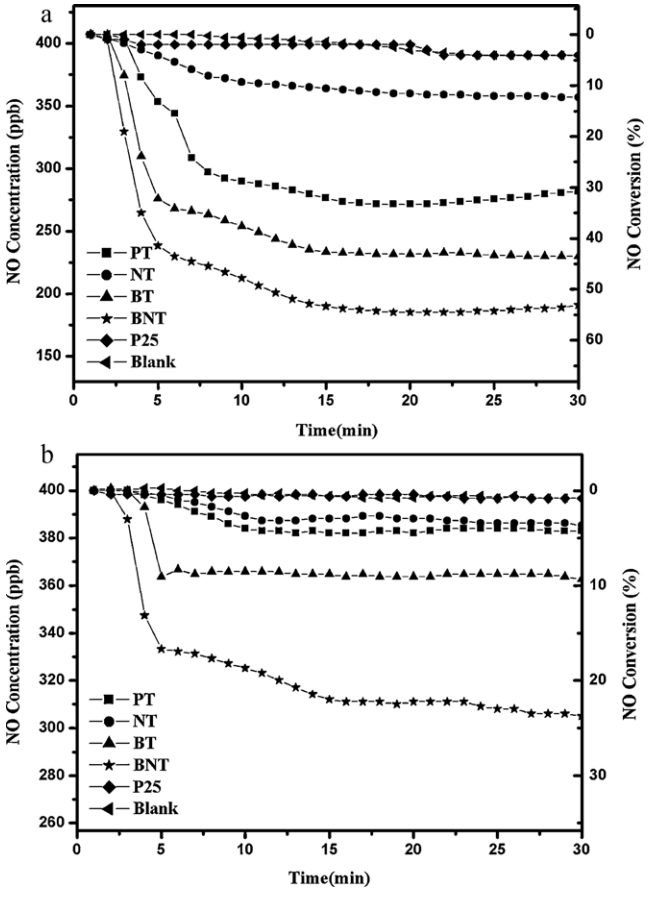

Fig. 7. NO concentration variation and conversion with the as-prepared samples under simulated solar light (a) and visible light (b) irradiation. Residence time: 3.72 min, humidity levels: 2200 ppmv.

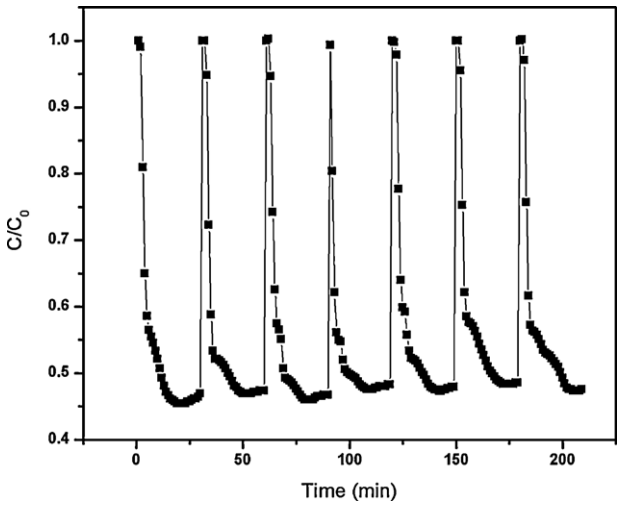

Fig. 8. The stability of BNT photocatalyst in multiple runs of degradation of NO under simulated solar light.

Two reasons might account for poor visible light photoactivity of NT. First, the band gap of the as-prepared NT was 2.66 eV, which was much smaller than that of PT (2.91 eV) (Fig. 5). This result indicates that NT possessed a weak redox ability and a high energy level of the conduction band, which disfavor the production of active oxygen radicals like O_2^-, •OOH, and •OH. Second, different from aqueous-phase photocatalysis, the intermediates generated by photocatalysis would accumulate on the surface of the photocatalyst to deactivate the photocatalyst during the gas phase photocatalytic process. So the NT sample might be more easily inactivated in the gas phase than pure titania, resulting in its poor visible light photoactivity for gas phase photocatalysis.

The stability of a photocatalyst is a key issue for its practical application. To further test the stability of the BNT photocatalyst on photocatalytic NO removal, we carried out multiple runs of photocatalytic experiments with the used BNT photocatalyst (Fig. 8). The recycling test revealed that the BNT sample exhibited no significant decrease in activity after being used repetitively for 7 times. The photocatalytic NO removal efficiency of BNT just decreased from 53% at the first run to 51% at the seventh run, suggesting that the BNT sample was stable and reusable although slight deactivation also existed. The reusability of the BNT sample is much better than nonaqueous sol–gel synthesized BiOBr [47], which makes it promising for the practical air purification.

4. Conclusions

In this study, we successfully obtained B, N-codoped TiO_2 hollow microspheres by using an aerosol assisted flow synthetic approach.

The B, N-codoped TiO_2 exhibited enhanced photocatalytic activity in comparison with pure and single element doped counterparts. The photocatalytic activity enhancement of B, N-codoped TiO_2 could be attributed to its large surface area, abundant mesoporous structure, narrow band gap and the synergistic effect of boron and nitrogen dopants. The high stability and reusability of B, N-codoped TiO_2 on NO removal suggests these B, N-codoped TiO_2 hollow microspheres are very promising for air purification.

Acknowledgements

This work was supported by National Basic Research Program of China (973 Program) (Grant 2007CB613301), National Science Foundation of China (Grants 20977039, 21073069, and 91023010), Program for Distinguished Young Scientist of Hubei Province (2009CDA014), Program for Innovation Team of Hubei Province (2009CDA048), Self-Determine Research Funds of CCNU from the Colleges' Basic Research and Operation of MOE (Grants CCNU09A02014 and CCNU09C01009), and Program for New Century Excellent Talents in University (Grant NCET-07-0352), and Program for Changjiang Scholars and Innovative Research Team in University (Grant IRT0953).

Appendix A. Supplementary data

Supplementary data associated with this article can be found, in the online version, at doi:10.1016/j.jhazmat.2011.03.099.

References

[1] F.B. Li, X.Z. Li, C.H. Ao, M.F. Hou, S.C. Lee, Photocatalytic conversion of NO using TiO_2–NH_3 catalysts in ambient environment, Appl. Catal. B: Environ. 54 (2004) 275–283.
[2] L.S.R. Brickus, J.N. Cardoso, F.R. de Aquino Neto, Distributions of indoor and outdoor air pollutants in Rio de Janeiro Brazil: implications to indoor air quality in bayside offices, Environ. Sci. Technol. 32 (1998) 3485–3490.
[3] S. Yin, B. Liu, P.L. Zhang, T. Morikawa, K. Yamanaka, T. Sato, Photocatalytic oxidation of NOx under visible LED light irradiation over nitrogen-doped titania particles with iron or platinum loading, J. Phys. Chem. C 112 (2008) 12425–12431.
[4] M.A. Fox, M.T. Dulay, Heterogeneous photocatalysis, Chem. Rev. 93 (1993) 341–357.
[5] A.L. Linsebigler, G.Q. Lu, J.T. Yates, Photocatalysis on TiO_2 surfaces: principles, mechanisms, and selected results, Chem. Rev. 95 (1995) 735–758.
[6] M. Anpo, M. Takeuchi, The design and development of highly reactive titanium oxide photocatalysts operating under visible light irradiation, J. Catal. 216 (2003) 505–516.
[7] R.L. Putnam, N. Nakagawa, K.M. McGrath, N. Ya, I.A. Aksay, S.M. Grune, A. Navrotsky, Titanium dioxide-surfactant mesophases and Ti-TMS1, Chem. Mater. 9 (1997) 2690–2693.
[8] V. Brezova, A. Blazkova, L. Karpinsky, J. Groskova, B. Havlinova, V. Jorik, M. Ceppan, Phenol decomposition using M^{n+}/TiO_2 photocatalysts supported by the sol–gel technique on glass fibres, J. Photochem. Photobiol. A: Chem. 109 (1997) 177–183.
[9] W. Choi, A. Termin, M.R. Hoffmann, The role of metal ion dopants in quantum-sized TiO_2: correlation between photoreactivity and charge carrier recombination dynamics, J. Phys. Chem. B 98 (1994) 13669–13679.
[10] R. Asahi, T. Morikawa, T. Ohwaki, K. Aoki, Y. Taga, Visible-light photocatalysis in nitrogen-doped titanium oxides, Science 293 (2001) 269–271.
[11] C. Burda, Y. Lou, X. Chen, A.C.S. Samia, J. Stout, J.L. Gole, Enhanced nitrogen doping in TiO_2 nanoparticle, Nano Lett. 3 (2003) 1049–1051.
[12] J.H. Park, S. Kim, A.J. Bard, Novel carbon-doped TiO_2 nanotube arrays with high aspect ratios for efficient solar water splitting, Nano Lett. 6 (2006) 24–28.
[13] C. Lettmann, K. Hildenbrand, H. Kisch, W. Wacyk, W.F. Maier, Visible light photodegradation of 4-chlorophenol with a coke-containing titanium dioxide photocatalyst, Appl. Catal. B: Environ. 32 (2001) 215–221.
[14] J.C. Yu, W.K. Ho, J.G. Yu, H.Y. Yip, P.K. Wong, J.C. Zhao, Efficient visible-light-induced photocatalytic disinfection on sulfur-doped nanocrystalline titania, Environ. Sci. Technol. 39 (2005) 1175–1179.
[15] X.T. Hong, Z.P. Wang, W.M. Cai, F. Lu, J. Zhang, Y.Z. Yang, N. Ma, Y.J. Liu, Visible-light-activated nanoparticle photocatalyst of iodine-doped titanium dioxide, Chem. Mater. 17 (2005) 1548–1552.
[16] H. Wang, J.P. Lewis, Second-generation photocatalytic materials: anion-doped TiO_2, J. Phys. Condens. Matter 18 (2006) 421–434.
[17] W. Zhao, W.H. Ma, C.C. Chen, J.C. Zhao, Z.G. Shuai, Efficient degradation of toxic organic pollutants with $Ni_2O_3/TiO_{2-x}B_x$ under visible irradiation, J. Am. Chem. Soc. 126 (2004) 4782–4783.
[18] S. In, A. Orlov, R. Berg, F. Garcia, S. Pedrosa-Jimenez, M.S. Tikhov, D.S. Wright, R.M. Lambert, Effective visible light-activated B-doped and B N-codoped TiO_2 photocatalysts, J. Am. Chem. Soc. 129 (2007) 13790–13791.
[19] D.M. Chen, D. Yang, Q. Wang, Z.Y. Jiang, Effects of boron doping on photocatalytic activity and microstructure of titanium dioxide nanoparticles, Ind. Eng. Chem. Res. 45 (2006) 4110–4116.
[20] M. Bettinelli, V. Dallacasa, D. Falcomer, P. Fornasiero, V. Gombac, T. Montini, L. Roman'o, A. Speghini, Photocatalytic activity of TiO_2 doped with boron and vanadium, J. Hazard. Mater. 146 (2007) 529–534.
[21] M. Fittipaldi, V. Gombac, T. Montini, P. Fornasiero, M. Graziani, A high-frequency (95 GHz) electron paramagnetic resonance study of B-doped TiO_2 photocatalysts, J. Phys. Chem. C 361 (2008) 3980–3987.
[22] E. Finazzi, C.D. Valentin, G. Pacchioni, Boron-doped anatase TiO_2: pure and hybrid DFT calculations, J. Phys. Chem. C 113 (2009) 220–228.
[23] Y. Cong, F. Chen, J.L. Zhang, M. Anpo, Carbon and nitrogen-codoped TiO_2 with high visible light photocatalytic activity, Chem. Lett. 35 (2006) 800–801.
[24] H.Q. Sun, Y. Bai, Y.P. Cheng, W.Q. Jin, N.P. Xu, Preparation and characterization of visible-light-driven carbon-sulfur-codoped TiO_2 photocatalysts, Ind. Eng. Chem. Res. 45 (2006) 4971–4976.
[25] D. Li, H. Haneda, S. Hishita, N. Ohashi, Visible-light-driven N-F-codoped TiO_2 photocatalysts. 1. Synthesis by spray pyrolysis and surface characterization, Chem. Mater. 17 (2005) 2588–2595.
[26] D. Li, H. Haneda, S. Hishita, N. Ohashi, Visible-light-driven N-F-codoped TiO_2 photocatalysts. 2. Optical characterization, photocatalysis, and potential application to air purification, Chem. Mater. 17 (2005) 2596–2602.
[27] Y.L. Su, X.W. Zhang, S. Han, X.Q. Chen, L.C. Lei, F–B-codoping of anodized TiO_2 nanotubes using chemical vapor deposition, Electrochem. Commun. 9 (2007) 2291–2298.
[28] Y.W. Wang, Y. Huang, Y.K. Ho, L.Z. Zhang, Z.G. Zou, S.C. Lee, Biomolecule-controlled hydrothermal synthesis of C–N–S-tridoped TiO_2 nanocrystalline photocatalysts for NO removal under simulated solar light irradiation, J. Hazard. Mater. 169 (2009) 77–87.
[29] V. Gombac, L. De Rogatis, A. Gasparotto, G. Vicario, P. Fornasiero, TiO_2 nanopowders doped with boron and nitrogen for photocatalytic applications, Chem. Phys. 339 (2007) 111–123.
[30] Q.C. Ling, J.Z. Sun, Q.Y. Zhou, Preparation and characterization of visible-light-driven titania photocatalyst co-doped with boron and nitrogen, Appl. Surf. Sci. 254 (2008) 3236–3241.
[31] N.O. Gopal, H.H. Lo, S.C. Ke, Chemical state and environment of boron dopant in B N-codoped anatase TiO_2 nanoparticles: an avenue for probing diamagnetic dopants in TiO_2 by electron paramagnetic resonance spectroscopy, J. Am. Chem. Soc. 130 (2008) 2760–2761.
[32] G. Liu, Y.N. Zhao, C.H. Sun, F. Li, G.Q. Lu, H.M. Cheng, Synergistic effects of B/N doping on the visible-light photocatalytic activity of mesoporous TiO_2, Angew. Chem. Int. Ed. 47 (2008) 4516–4520.
[33] G.L. Messing, S. Zhang, G.V. Jayanthi, Ceramic powder synthesis by spray pyrolysis, J. Am. Ceram. Soc. 76 (1993) 2707–2726.
[34] D. Li, N. Ichikuni, S. Shimazu, T. Uematsu, Hydrogenation of CO_2 over sprayed Ru/TiO_2 fine particles and strong metal–support interaction, Appl. Catal. A: Gen. 180 (1999) 227–235.
[35] X. Song, X. Ding, P.N. Li, Z.H. Ai, L.Z. Zhang, H_3BO_3-induced formation of metal oxide hollow spheres in the flowing aerosols, J. Phys. Chem. C 113 (2009) 5455–5459.
[36] Y. Huang, W.K. Ho, Z.H. Ai, X. Song, L.Z. Zhang, S.C. Lee, Aerosol-assisted flow synthesis of B-doped Ni-doped and B–Ni-codoped TiO_2 solid and hollow microspheres for photocatalytic removal of NO, Appl. Catal. B: Environ. 89 (2009) 398–405.
[37] K.Y. Jung, S.B. Park, S.K. Ihm, Local structure and photocatalytic activity of B_2O_3–SiO_2/TiO_2 ternary mixed oxides prepared by sol–gel method, Appl. Catal. B: Environ. 51 (2004) 239–245.
[38] T.C. Jagadale, S.P. Takale, R.S. Sonawane, B.B. Kale, S.I. Patil, S. Ogale, N-doped TiO_2 nanoparticle based visible light photocatalyst by modified peroxide sol–gel method, J. Phys. Chem. C 112 (2008) 14595–14602.
[39] K.S.W. Sing, D.H. Everett, R.A.W. Haul, L. Moscou, R.A. Pierotti, J. Rouquerol, T. Siemieniewska, Reporting physisorption data for gas/solid systems with special reference to the determination of surface area and porosity, Pure Appl. Chem. 57 (1985) 603–619.
[40] N.D. Feng, A.M. Zheng, Q. Wang, P.P. Ren, X.Z. Gao, S.B. Liu, Z.R. Shen, T.H. Chen, F. Deng, Boron environments in B-doped and (B N)-codoped TiO_2 photocatalysts: a combined solid-state NMR and theoretical calculation study, J. Phys. Chem. C 115 (2011) 2709–2719.
[41] X.B. Chen, C. Burda, Photoelectron spectroscopic investigation of nitrogen-doped titania nanoparticles, J. Phys. Chem. B 108 (2004) 15446–15449.
[42] Y. Cong, J.L. Zhang, F. Chen, M. Anpo, Synthesis and characterization of nitrogen-doped TiO_2 nanophotocatalyst with high visible light activity, J. Phys. Chem. C 111 (2007) 6976–6982.
[43] M. Grunze, C.R. Brundle, D. Tománek, Adsorption and decomposition of ammonia on a W(1 1 0) surface: photoemission fingerprinting and interpretation of the core level binding energies using the equivalent core approximation, Surf. Sci. 119 (1982) 133–149.
[44] H. Choi, M. Antoniou, M. Pelaez, D. Dionysiou, J. Shoemaker, Mesoporous nitrogen-doped TiO_2 for the photocatalytic destruction of the cyanobacterial toxin microcystin-LR under visible light irradiation, Environ. Sci. Technol. 41 (2007) 7530–7535.
[45] N.C. Saha, H.G. Tompkins, Titanium nitride oxidation chemistry: an X-ray photoelectron spectroscopy study, J. Appl. Phys. 72 (1992) 3072–3079.

[46] F. Dong, H.Q. Wang, Z.B. Wu, One-step "green" synthetic approach for mesoporous C-doped titanium dioxide with efficient visible light photocatalytic activity, J. Phys. Chem. C 113 (2009) 16717–16723.
[47] Z.H. Ai, W.K. Ho, S.C. Lee, L.Z. Zhang, Efficient photocatalytic removal of NO in indoor air with hierarchical bismuth oxybromide nanoplate microspheres under visible light, Environ. Sci. Technol. 43 (2009) 4143–4150.
[48] J.C. Yu, L.Z. Zhang, J.G. Yu, Direct sonochemical preparation and characterization of highly active mesoporous TiO_2 with a bicrystalline framework, Chem. Mater. 14 (2002) 4647–4653.
[49] S. Bo, G.S. Panagiotis, Interaction of anatase and rutile TiO_2 particles in aqueous photooxidation, Catal. Today 88 (2003) 49–59.
[50] S.H. Kim, W.Y. Choi, Visible-light-induced photocatalytic degradation of 4-chlorophenol and phenolic compounds in aqueous suspension of pure titania: demonstrating the existence of a surface-complex-mediated path, J. Phys. Chem. B 109 (2005) 5143–5149.
[51] Y.W. Wang, L.Z. Zhang, K.J. Deng, X.Y. Chen, Z.G. Zou, Low temperature synthesis and photocatalytic activity of rutile TiO_2 nanorod superstructures, J. Phys. Chem. C 111 (2007) 2709–2714.
[52] S.C. Moon, H. Mametsuka, T. Soichi, E. Suzuki, Photocatalytic production of hydrogen from water using TiO_2 and B/TiO_2, Catal. Today 58 (2000) 125–132.
[53] C.D. Valentin, E. Finazzi, G. Pacchioni, Density functional theory and electron paramagnetic resonance study on the effect of N–F codoping of TiO_2, Chem. Mater. 20 (2008) 3706–3714.